The Alrestatin Double-Decker: Binding of Two Inhibitor Molecules to Human Aldose Reductase Reveals a New Specificity Determinant†

David H. T. Harrison,*,‡,§ Kurt M. Bohren,|| Gregory A. Petsko,‡ Dagmar Ringe,‡ and Kenneth H. Gabbay*,||

Rosenstiel Basic Medical Sciences Research Center, Brandeis University, Waltham, Massachusetts 02554, and Molecular Diabetes & Metabolism Section, Department of Pediatrics, Baylor College of Medicine, Houston, Texas 77030

Received July 14, 1997; Revised Manuscript Received October 15, 1997⊗

ABSTRACT: It is generally expected that only one inhibitor molecule will bind to an enzyme active site. In fact, specific drug design theories depend upon this assumption. Here, we report the binding of two molecules of an inhibitor to the same active site which we observed in the 1.8 Å resolution structure of the drug Alrestatin bound to a mutant of human aldose reductase. The two molecules of Alrestatin bind to the active site in a stacked arrangement (a double-decker). This stack positions the carboxylic acid of one drug molecule near the $NADP^+$ cofactor at a previously determined anion binding site and the carboxylic acid of the second drug molecule near the carboxy-terminal tail of the enzyme. We propose that interactions of inhibitors with the carboxy-terminal loop of aldose reductase are critical for the development of inhibitors that are able to discriminate between aldose reductase and other members of the aldo−keto reductase superfamily. This finding suggests a new direction for the introduction of specificity to aldose reductase-targeted drugs.

Aldose reductase catalyzes the NADPH-dependent reduction of an aldehyde or short-chain ketone to its corresponding alcohol. This activity contributes to the development of diabetic complications by mediating the conversion of excess glucose (an aldehyde) to sorbitol (an alcohol) in the first step of the polyol pathway. The three-dimensional structure of human aldose reductase (EC 1.1.1.21) has been determined at high resolution (*1, 2*), and a detailed mechanism has been proposed for its NADPH-dependent activity (*3*). Aldose reductase is an α/β barrel that consists of eight β-strands forming the inside of the barrel and ten α-helices surrounding the barrel. Additionally, there are two β-strands that form the bottom of the barrel. An $NADP^+$ cofactor lies in an extended conformation across the barrel, with its nicotinamide ring lying at the bottom of a large cavity near the top of the barrel to form the active site. In the oxidized ($NADP^+$) form of aldose reductase, an anion binding site is formed at a point that is nearly equidistant (∼2.8 Å) from the C4 carbon of the nicotinamide ring, the OH oxygen of tyrosine 48, and the Nϵ2 nitrogen of histidine 110. This region of the active site is responsible for the protonation of the oxygen atom of the substrate during catalysis. Aldose reductase proceeds by an ordered bi-bi reaction mechanism whereby binding of NADPH precedes the binding of the aldehyde substrate, and the release of $NADP^+$ is the final step in the catalytic cycle. The overall catalytic mechanism is best described in either direction by the enzyme binding to the nucleotide substrate, a subsequent conformational change of the enzyme followed by the binding of the aldehyde/alcohol substrate and the transfer of a proton and a hydride. Detailed analysis of each of these steps reveals that the conformational changes associated with the exchange of $NADP^+$ for NADPH are the rate-determining step of the overall reaction (*4, 5*).

Although the pathogenesis of diabetic complications remains unclear, an increased flux of glucose through aldose reductase and the polyol pathway can cause the development of the diabetic complications of neuropathy, nephropathy, and retinopathy (*6, 7*). To prevent these complications, a large number of aldose reductase inhibitors have been developed. Alrestatin is the first orally effective and clinically investigated inhibitor of aldose reductase (*8*−*10*). Despite the efficacy of some aldose reductase inhibitors in preventing sugar-induced cataracts in animal models, these inhibitors have proven to be either ineffective or toxic in clinical trials (*11, 12*). A possible explanation for the toxicity of these compounds is that they do not adequately discriminate between aldose reductase and other related enzymes. This view is supported by the fact that aldose reductase is part of the aldo−keto reductase superfamily which includes such enzymes as aldehyde reductase and prostaglandin F synthase (*12*). As part of an effort to better understand the specificity of aldose reductase inhibitors, we studied the interaction of Alrestatin with a series of mutants of aldose reductase. Unlike wild-type aldose reductase, one of these mutant aldose reductase proteins formed diffraction-quality crystals. We herein report the structure of two Alrestatin molecules bound as a double-decker in the active site of a double mutant W219Y/C298A of human aldose reductase.

METHODS

Protein Expression and Purification. Mutations were introduced into the human aldose reductase cDNA to give the double mutant W219Y/C298A (to be published elsewhere). The mutant aldose reductase protein was expressed using a pET vector in *Escherichia coli* and purified as previously described (*13*).

† This work was supported by grants from the National Institutes of Health, DK-51697, GM-26788, and EY-11018, the Juvenile Diabetes Foundation, the Lucille P. Markey Charitable Trust, and the Harry B. and Aileen B. Gordon Foundation.

* Corresponding authors.

‡ Brandeis University.

§ Current address: Department of Biochemistry, Medical College of Wisconsin, Milwaukee, WI 53226-0509.

|| Baylor College of Medicine.

⊗ Abstract published in *Advance ACS Abstracts,* December 1, 1997.

S0006-2960(97)01713-3 CCC: $14.00

Enzyme Assays and Enzyme Analysis. Enzymatic activities were assayed during purification by measuring the rate of the enzyme-dependent decrease of NADPH absorption at 340 nm in a Gilford Response spectrophotometer at 25 °C. The standard reaction mixture (1 mL volume) contained 0.2 mM NADPH and 1 or 5 mM DL-glyceraldehyde, depending on the wild-type or the mutant enzyme being analyzed, in a 100 mM sodium phosphate buffer, pH 7. Kinetic constants were determined in the same way except for varying the substrate concentrations. Each data point (initial velocity) was determined in duplicate over at least five different substrate concentrations. Control assays, lacking either substrate or enzyme, were routinely included, and the rates, if any, were subtracted from the reaction rates. Kinetic constants were calculated by fitting the Michaelis−Menten function directly in the hyperbolic form to the data with an unweighted least-squares analysis using the Marquardt−Levenberg algorithm provided with SigmaPlot for Windows, version 2.0. Steady-state kinetics in the presence of inhibitors were analyzed by using the equation $v_i = VA/[K_m(1 + I/K_{is}) + A(1 + I/K_{ii})]$, where K_{is} is the slope (competitive) inhibitory constant and K_{ii} is the intercept (uncompetitive) inhibition constant. The inhibition pattern and a >5-fold relative difference between K_{is} and K_{ii} determined competitive or uncompetitive inhibition. Accordingly, either term in the equation was set to 1, and the fit for either K_{is} or K_{ii} improved significantly as judged from the standard errors and the sum of the residual least-squares values. The kinetic nomenclature used is that of Cleland (*14*).

Crystallization. Mutant aldose reductase crystals were obtained at 4 °C as described earlier (*1, 2*) by the hanging-drop vapor diffusion method. The "well" solution contained between 15% and 20% (w/w) poly(ethylene glycol) (PEG 6000). The "drop" contained protein (14 mg/mL) and half the well amount of PEG 6000 in a buffer containing 25 mM sodium citrate (pH 5.0), 7 mM β-mercaptoethanol, 1 mM $NADP^+$, and 1 mM Alrestatin and a C298A mutant "seed" crystal. Citrate-bound crystals were also produced by incubation of the mutant enzyme in 100 mM sodium citrate (pH 5.0) without Alrestatin.

Model Making. Models of Alrestatin bound to the active site of aldose reductase were made using the program QUANTA.

Data Collection and Processing. Oscillation data were collected on a Siemens multiwire area detector (X100A) using nickel-filtered Cu Kα radiation from an Elliot GX-6 rotating anode running at 30 kV × 25 mA. The crystal to detector distance was kept at 100 mm, and a Lorentz/polarization-corrected data set was created by processing the images with XDS and XSCALE (*15*).

Crystallographic Refinement. Initial phases were calculated by X-PLOR (*16*) from the native structure without water molecules or citrate present. After rigid body refinement of the protein and $NADP^+$ cofactor, the *R*-factor was 25% at 2.5 Å resolution. The initial electron density map showed that two molecules of Alrestatin had bound to the active site. Parameter and PSF files for refinement of the Alrestatin molecules were determined using QUANTA. Using the program O (*17*), the first Alrestatin molecule was fit into the electron density. This model had a free *R*-factor of 28.0% and an *R*-factor of 23.0% at 1.8 Å resolution. After the addition of 100 water molecules and positional refinement, the free *R*-factor dropped to 23.5% with an *R*-factor of 18.8%. At this point the second Alrestatin molecule was clearly present. Adding the second Alrestatin and further rounds of manual rebuilding and refinement lowered the free *R*-factor to 23.2% and the *R*-factor to 17.7%.

Table 1: Kinetic and Inhibition Constants Obtained for Wild-Type and W219Y/C298A Mutant Aldose Reductase Using DL-Glyceraldehyde as a Substrate

		wild type	W219Y/C298A	aldehyde reductase[a]
DL-glyceraldehyde	k_{cat} (s^{-1})	0.5 ± 0.05	1.0 ± 0.05	
	K_m (mM)	0.02 ± 0.002	0.17 ± 0.01	
	k_{cat}/K_m (mM^{-1} s^{-1})	25.0 ± 5.0	5.6 ± 0.3	
Alrestatin	K_{is} (μM)	2.0 ± 0.1	38 ± 18	148 ± 12
	K_{ii} (μM)	2.0 ± 0.1	7.5 ± 0.4	148 ± 12
citrate	K_i (μM)	9400 ± 600	58000 ± 3000	

[a] Data obtained from Barski *et al.* (*22*).

RESULTS

Enzyme Kinetics and Inhibition Mechanism. Some apparent kinetic parameters of the double mutant W219Y/C298A were determined to assess the validity of using this mutant to investigate the binding of Alrestatin to the wild-type enzyme. Table 1 shows that the k_{cat}/K_m for the double mutant is less than 5 times lower than that of the wild-type enzyme. Thus, it is unlikely that this enzyme proceeds by a different kinetic mechanism or that the active site is changed with respect to DL-glyceraldehyde. Further evidence supporting the use of the mutant enzyme as a model for the wild-type enzyme is found in the small perturbation of the inhibition constants for citrate and Alrestatin. The 6- and 3-fold increases in the uncompetitive binding constants for citrate and Alrestatin, respectively, suggest little structural change in the oxidized ($NADP^+$) form of the enzyme as compared to the wild-type enzyme. The increase in the competitive portion of the binding constant K_{is} for the mutant enzyme may suggest that the reduced (NADPH) form of the mutant does not bind the inhibitor as tightly as the wild-type enzyme. This may be correlated with the increase in the apparent K_m for the substrate, which includes both microscopic rate constants as well as substrate binding constants. The reduction kinetics of aldose reductase predict that binding of an inhibitor that binds equally tight to the E·NADPH and E·$NADP^+$ forms of the enzyme produces inhibition constants K_{is} and K_{ii} of equal values. Thus, relative differences in binding strength to either complex are reflected in the values of the respective constant. However, since our crystallographic investigations are of the oxidized ($NADP^+$) form of the enzyme, this 10-fold change in K_{is} may not have much bearing on our conclusions. Together, these data suggest that the structure of the Alrestatin complex with the mutant enzyme is likely to be representative of the Alrestatin complex with the wild-type enzyme.

Model Making. Alrestatin can be considered a pharmacophore in which a terminal negatively charged oxygen is found three atoms away from a large aromatic ring system (AR1/AR2, Figure 1). Most commercially developed aldose reductase inhibitors contain this pharmacophore, either as a spirohydantoin or as ring system derivatives of acetic acid. Thus, in order to gain an understanding of the interaction of this pharmacophore with aldose reductase, we modeled Alrestatin into the active site. The model of Alrestatin bound

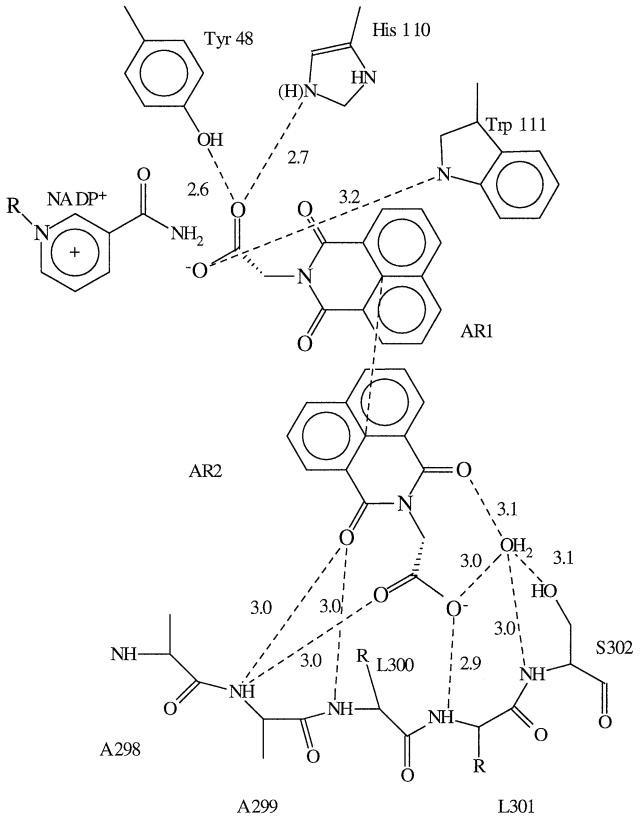

FIGURE 1: Schematic diagram of the two molecules of Alrestatin (AR1, AR2) bound to the active site of aldose reductase. The two molecules are stacked 3.7 Å apart, forming the "Alrestatin double-decker".

to the active site of aldose reductase was constructed using a number of structural and electronic (charge, bond order, hybridization, etc.) principles derived from crystal structures of AR complexed with other inhibitors (*1*, *18*).

We positioned the carboxylate of the Alrestatin molecule in the previously identified anion binding site (*1*). Fluorescence quenching studies of the aldose reductase−Alrestatin complex provide experimental evidence of a stacking interaction between a molecule of Alrestatin and the indole ring of Trp20 (*19*). Consequently, the ring system of Alrestatin was positioned in the model so as to stack against this tryptophan. This model for Alrestatin binding is similar to the mode of drug binding observed in the crystal structure of the inhibitor Zopolrestat bound to aldose reductase (*18*). The primary structural difference between the Zopolrestat complex and the Alrestatin model was a steric conflict between a portion of Alrestatin and Trp219, which is due to differences in the geometries of the ring systems in these two drugs. We predicted that the backbone atoms of Trp219 would move to accommodate Alrestatin. This prediction relied in part on the observation that Trp219 is at the N-terminus of a postulated flexible loop found in the aldose reductase crystal structure (*1*, *2*).

Structure Determination. All attempts to crystallize Alrestatin with wild-type aldose reductase have so far failed. The aldose reductase double mutant W219Y/C298A was crystallized in the presence of either citrate or Alrestatin as described in the Methods section. These crystals were difficult to obtain as compared to the wild-type enzyme, and they diffracted to a resolution of 2.9 and 1.8 Å, respectively. Since the crystals were isomorphous with wild-type crystals, initial phases were calculated with the wild-type structure

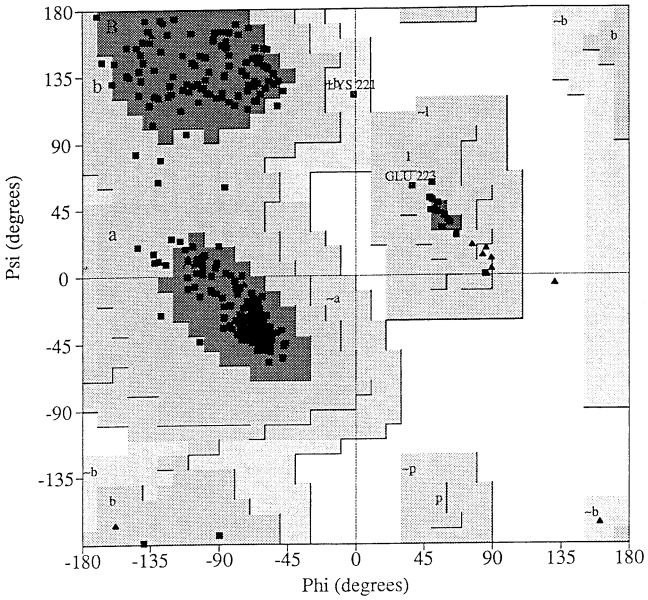

FIGURE 2: Ramachandran plot of aldose reductase bound to Alrestatin. Only the highly disordered residues Lys221 and Glu223 are not in the allowed region of the plot.

Table 2: Crystallographic Data for the Alrestatin−$NADP^+$−W219Y/C298A and Citrate−$NADP^+$−W219Y/C298A Mutant Aldose Reductase Complex

	Alrestatin−$NADP^+$−W219Y/C298A	citrate−$NADP^+$−W219Y/C298A
unit cell parameters		
a (Å)	49.96	50.30
b (Å)	67.07	67.20
c (Å)	92.19	92.30
collection statistics		
resolution range (last shell)	10−1.8 (1.9−1.8)	10−2.90 (3.03−2.9)
obsd reflections (shell)	87251 (6429)	31641 (4819)
unique reflections (shell)	26959 (3134)	7308 (1288)
R-merge (%)	7.5 (33.5)	12.8 (22.5)
refinement statistics		
working		
reflections ($I > 2\sigma$) (shell)	23059 (1973)	5965 (746)
completeness (%)	79.0 (55.1)	93.2 (89.2)
working *R*-factor	0.177 (0.252)	0.196 (0.230)
free		
reflections ($I > 2\sigma$) (shell)	2526 (194)	0 (0)
completeness (%)	8.6 (5.4)	0 (0)
free *R*-factor	0.232 (0.306)	NA
no. of atoms		
protein	2509	2509
$NADP^+$	48	48
Alrestatin	38	38
water	220	0
RMS deviation from ideality		
bond length (Å)	0.012	0.018
bond angles (deg)	1.354	1.826
bond dihedrals (deg)	25.68	27.68
planarity (deg)	2.016	2.55

[a] Structures deposited in the Protein Data Bank (1az1 and 1az2).

mutated at residues 219 and 298 with neither solvent nor inhibitor present. Rigid body refinement gave rise to electron density which could immediately be interpreted. The Alrestatin-bound structure required rebuilding of the residues around residue Trp 219 whereas the citrate bound structure did not. A Ramachandran plot of the Alrestatin complex with the mutant enzyme is shown (Figure 2) as are the refinement statistics for both the Alrestatin complex and the citrate complex (Table 2).

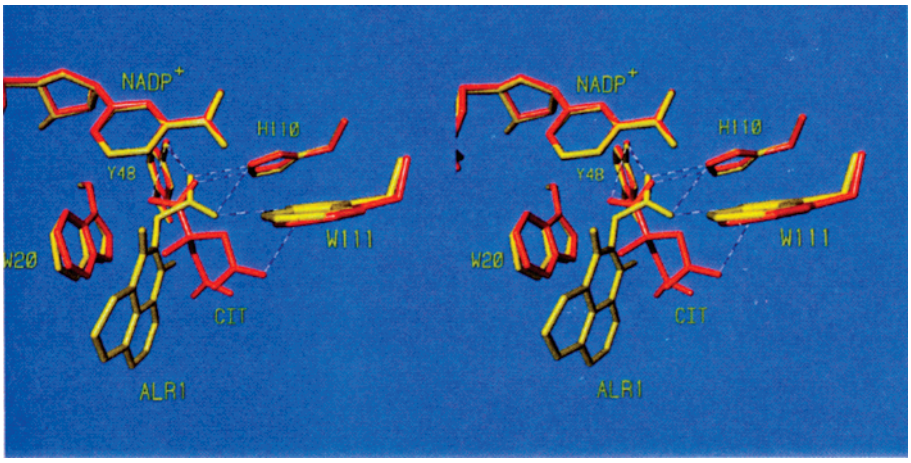

FIGURE 3: Three-dimensional view of the active site comparing the structure of the wild-type protein with citrate (CIT) bound (red) to that of the mutant protein with one of the bound Alrestatin molecules (ALR1) (yellow). Note that the carboxylate of the citrate molecule is directed toward the hydroxyl of tyrosine 48 and the carboxylate of the Alrestatin molecule is directed toward the Nϵ2 nitrogen of histidine 110. Also note that both inhibitors form hydrogen bonds with tryptophan 111.

As predicted in the model, the crystal structure shows that the ring of one Alrestatin molecule is stacked 3.7 Å from the indole ring of Trp20. Also as predicted, the carboxylic acid moiety of this molecule is bound in the anion binding site. Figure 3 shows the three-dimensional interactions of the "AR1" molecule of Alrestatin with the residues in the active site. The similarity to citrate binding is striking; both inhibitors are capable of forming hydrogen bonds to Tyr48, His110, Trp111, and the amide on the nicotinamide ring. However, the carboxylates are aligned quite differently; the citrate carboxylate points toward the hydroxyl of Tyr48, while the carboxylate of Alrestatin points toward His110. This change in direction is most easily explained by the stacking interaction between Alrestatin and Trp20. Interestingly, the side chain of Trp20 has moved 0.6 Å to accommodate the Alrestatin molecule. This movement may be linked to the fact that the carboxylate of Alrestatin is bound closer to the hydroxyl of Tyr48 than is the citrate carboxylate. The proximity of the carboxyl carbon of Alrestatin to the C4 carbon of $NADP^+$ suggests that Alrestatin may be a better mimic of the transition state for hydride transfer than is citrate.

A Second Alrestatin Molecule. Remarkably, the X-ray crystal structure of the Alrestatin complex shows a second Alrestatin molecule bound to the active site of the mutant aldose reductase (Figure 4a). The modeling studies did not predict the binding of a second Alrestatin molecule because simultaneous binding of two drug molecules to the same active site is unprecedented. Figure 4b shows the spatial orientation of the pair of stacked Alrestatin molecules (which we term the Alrestatin double-decker) in relation to the other residues in the active site. One face of the second Alrestatin ring system is stacked 3.7 Å away from the ring system of the first molecule, while the other face is in van der Waals contact with Leu300. This arrangement fills nearly the entire active site pocket with inhibitor atoms (Figure 5). This tight fit allows the second Alrestatin molecule to exclude four ordered water molecules not displaced when the smaller inhibitor citrate is bound. The second Alrestatin molecule is rotated 120° about the center of the ring system relative to the first Alrestatin molecule, and the carboxylic acid of the second Alrestatin molecule is oriented toward the same side of the ring system as that of the first molecule. One of the imide carbonyl oxygens and one of the carboxylic acid oxygens act as direct hydrogen bond acceptors for the backbone amide nitrogen of residue Ala299. The other carboxylic acid oxygen polarizes a bound water molecule, which in turn acts as a hydrogen bond acceptor for the backbone amide nitrogens of residues Leu301 and Ser302.

In the aldose reductase used in these experiments, Trp219 and Cys298 were mutated to tyrosine and alanine, respectively. In this mutant structure, the flexible nucleotide-holding loop adopts a somewhat different conformation and becomes even less well ordered. This change corresponds to a movement of the C_α of Tyr219 by 2.2 Å relative to the C_α of the tryptophan in the wild-type structure. Additionally, the tyrosine side chain adopts a different conformation than does the tryptophan in the wild-type structure. A 120° change in the χ_1 torsion angle (between C_α and C_β) of Tyr219 fully exposes this side chain to the solvent. To test if these changes are a property of the mutant enzyme or a property associated with Alrestatin binding, the mutant aldose reductase was crystallized in the presence of citrate. In this structure, the citrate molecule is bound to the active site in the same manner as it is in the wild-type complex. Further, this structure shows that the tyrosine remains in the same position and has the same χ_1 torsion angle as does the tryptophan in the corresponding wild-type structure (Figure 6).

DISCUSSION

The Alrestatin Complex Model Compared to Its X-ray Structure. The main features of the Alrestatin model described above were confirmed by the crystal structure of the Alrestatin−aldose reductase complex, which we have determined by cocrystallizing a mutant of human aldose reductase with Alrestatin. In our model, we predicted a change in the position of residue 219 and concluded that it should occur in response to Alrestatin, and not as an intrinsic property of the mutant. At this time, it is not possible to know the structure of the wild-type enzyme bound to Alrestatin. However, the similarity of the wild-type enzyme and the mutant enzyme with citrate bound suggests that the tryptophan of the wild-type enzyme would move analogously to the tyrosine when Alrestatin is bound. Some differences in the "flexible" loop (residues 219−225) of the mutant structure persist in the citrate-bound structure (although the

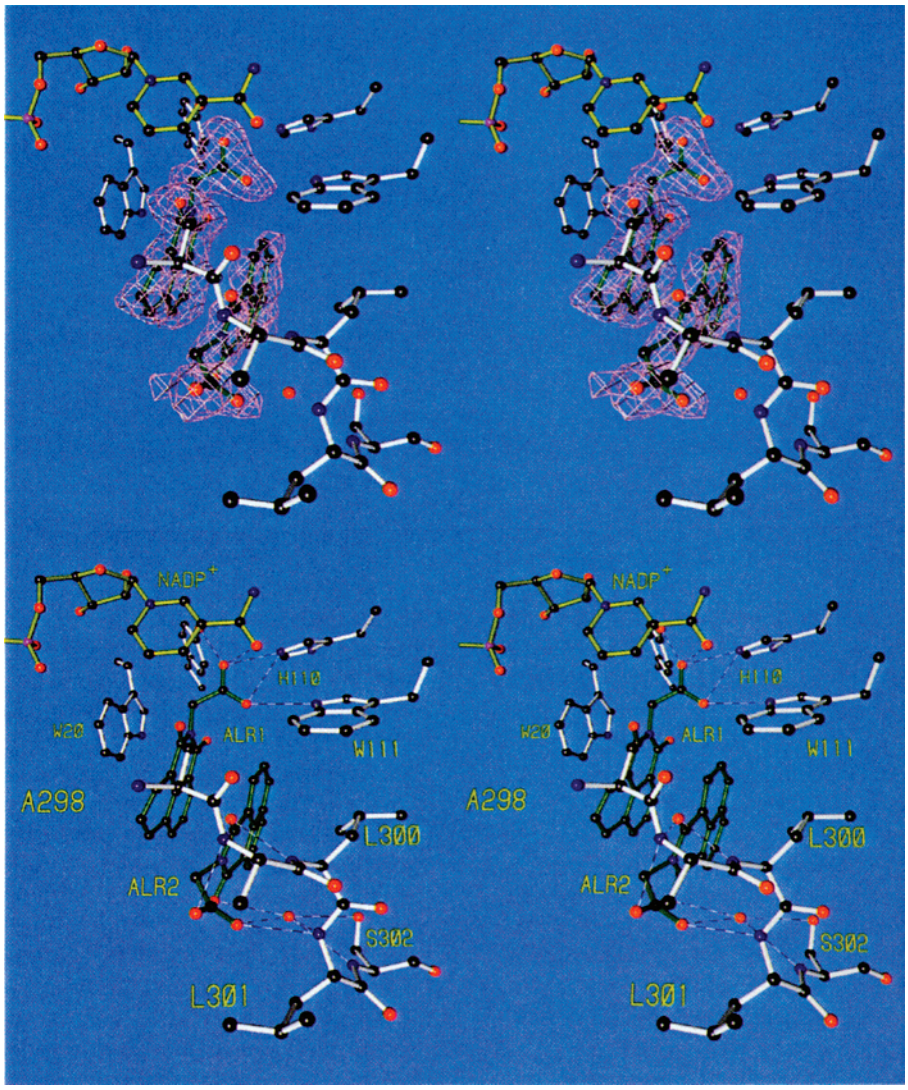

FIGURE 4: Three-dimensional view of the active site with bound Alrestatin. (a, top) Difference electron density map contoured at 2.5σ above the mean shows the presence of two Alrestatin molecules. The map was calculated using the refined coordinates prior to the addition of either Alrestatin molecule. (b, bottom) The final model based on our interpretation of the electron density shows the Alrestatin double-decker in the active site. Unattached red spheres represent water molecules found in the protein structure.

positions of these atoms are not well-defined due to their large temperature factors). It is interesting to note that Lys221 appears to make a weak hydrogen bond to Trp219 in the citrate-bound wild-type structure (3.4 Å) that is absent from the mutant enzyme. This missing hydrogen bond may lead to more flexibility in the loop region that may facilitate $NADP^+$/NADPH exchange. Alternatively, the elimination of the sulfur−aromatic interaction between Trp219 and Cys298 in this mutant may be responsible for the observed small increases in k_{cat}.

It is significant that the carboxylate of the unexpected second Alrestatin molecule is interacting with the backbone amides of the carboxy-terminal tail of aldose reductase. The composition of the amino acid sequence and length of the C-terminal tails of different members of the aldo−keto reductase superfamily are in large part responsible for the observed differences in their substrate and inhibitor specificities (*20, 21*). A chimeric protein consisting of the first 72 N-terminal residues from aldehyde reductase and the remaining residues from aldose reductase has aldose reductase substrate specificity, while deletion of the C-terminal tail of

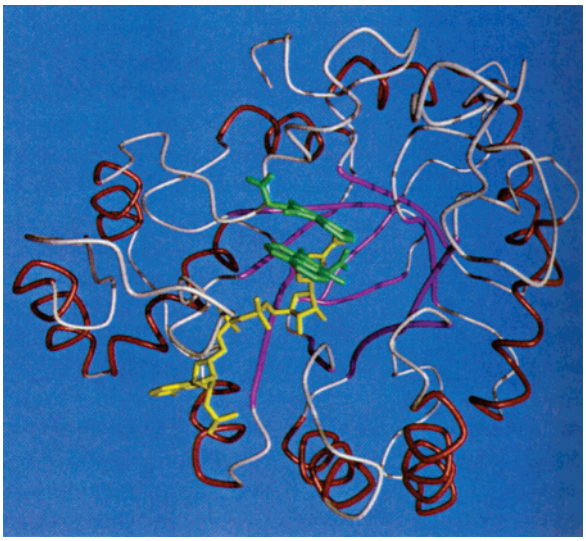

FIGURE 5: Wire representation of Alrestatin bound to aldose reductase. β-Sheets (magenta), α-helices (red), loops (gray), $NADP^+$ cofactor (yellow), and the two Alrestatin molecules (green) are shown in the active site which is at the carboxy-terminal side of the β-barrel.

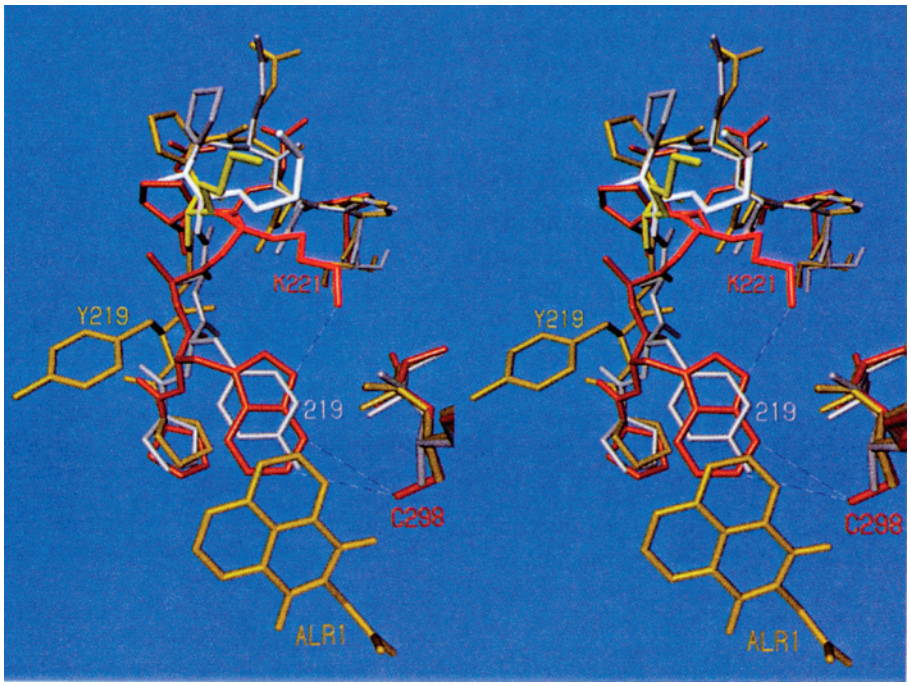

FIGURE 6: Three-dimensional view of the flexible loop region for the wild-type protein bound to citrate (red), the double mutant bound to citrate (white), and the double mutant bound to Alrestatin (yellow). The tyrosine and the tryptophan in the citrate-bound structures occupy the same part of space as the Alrestatin in the Alrestatin-bound structure. The tyrosine in the Alrestatin-bound structure is probably a good proxy for the tryptophan when Alrestatin is bound to the wild-type enzyme.

Table 3: Residues in the Active Site Cavity in Human Aldose Reductase (AR) and Their Human Homologues in Aldehyde Reductase (GR), Dihydrodiol Dehydrogenase Isozyme DD4 (DD-I4), Hepatic Bile Acid-Binding Protein (HBAP), and Cholestenone 5β-Reductase (C5BR) (*24*)

residue no.	AR	GR	DD-I4	HB AP	C5BR
20	Trp	Trp	Tyr	Tyr	Tyr
43	Asp	Asp	Asp	Asp	Asp
48	Tyr	Tyr	Tyr	Tyr	Tyr
77	Lys	Lys	Lys	Lys	Lys
79	Trp	Trp	Trp	Trp	Trp
110	His	His	His	His	His
111	Trp	Trp	Phe	Phe	Val
122	Phe	Phe	Leu	Ile	Tyr
159	Ser	Ser	Ser	Ser	Ser
160	Asn	Asn	Asn	Asn	Asn
183	Gln	Gln	Gln	Gln	Gln
209	Tyr	Tyr	His	Tyr	Tyr
218	Pro	Ala	Leu	Pro	Ile
219	Trp	Trp	Trp	Trp	Trp
298	Cys	Ile	Val	Leu	Val
299	Ala	Val	Val	Thr	Glu
300	Leu	Pro	Met	Leu	Leu
301	Leu	Met	Asp	Asp	Leu
302	Ser	Leu	Phe	Ile	Met

aldose reductase dramatically alters the substrate specificity (*21*). Recently, we showed that the preference of aldehyde reductase for carboxyl-containing substrates results from the unique presence of Arg311 in its C-terminal tail (*20*). An alignment of the five human aldo−keto reductase superfamily members (Table 3) shows that, of the residues located in the active site, Cys298, Ala299, Leu301, and Ser302 are among the least well conserved. We therefore postulate that the folding of the carboxy-terminal tails of the various aldo−keto reductases may be unique and characteristic of their specific amino acid composition. Thus, the geometry of the backbone amide nitrogens and carbonyl oxygens in this region may provide unique drug binding pockets that may impart specificity for each of the aldo−keto reductases.

Comparison to Zopolrestat Binding. This binding mode is dramatically different from the interactions that these same residues make with Zopolrestat. In the Zopolrestat complex, the C-terminal loop of aldose reductase moves more than 2.0 Å in order to accommodate the inhibitor, but the second Alrestatin molecule interacts with these C-terminal residues so as to displace them by less than 0.4 Å. Furthermore, unlike Zopolrestat, the second Alrestatin molecule is not stacked with the evolutionarily conserved Trp111. Although Zopolrestat binds rather differently than the Alrestatin double-decker, it exhibits many of the same binding characteristics. Both molecules place a carboxylate in the anion binding site, and both molecules also take advantage of ring stacking with Trp20. When Zopolrestat binds to the active site, the C-terminal residues are distorted, but there is energetic compensation by burying some of the hydrophobic surface area of these residues. It may be that these distortions are more difficult to make in other members of the aldo−keto reductase superfamily, thus giving Zopolrestat its selectivity for aldose reductase (*22*). The Alrestatin double-decker conforms better to the shape of the very large active site cavity of aldose reductase. The Alrestatin double-decker derives its selectivity for aldose reductase by making specific hydrogen bonds to the backbone of the same C-terminal loop of aldose reductase.

Implications for Future Drug Design. Although two Alrestatin molecules are found in the active site in this crystallographic study, it may be that at pharmacological levels of Alrestatin only one molecule binds to the active site. Interestingly, nonspecific multiadditions of inhibitor ligands to the aldose reductase holoenzyme were also found in a recent electrospray mass spectrometry study, where up to six adducts of Tolrestat were observed, only one molecule of which was bound tightly enough to qualify for binding to the active site (*23*). Given the similarity of the active site region where the "first" Alrestatin molecule binds, it is

difficult to explain Alrestatin's observed preference for binding aldose reductase over binding aldehyde reductase. Although there is no solution evidence for the observed second molecule, its presence would make differences in the inhibition constants easier to understand. Regardless, the importance of this structure is that it demonstrates that it should be possible to construct highly specific aldose reductase inhibitors that mimic the principles found in the Alrestatin double-decker. The Alrestatin double-decker shows the importance of simultaneously recognizing the carboxy-terminal tail of aldose reductase while filling the entire active site binding pocket by using a ring system that can exploit the stacking interactions with Trp20 and an appropriate negative charge to satisfy the anion binding site. Conventional drug design has mostly exploited the last two binding requirements. Unfortunately, while these two requirements appear to be necessary for inhibition of all members of the aldo−keto reductase superfamily, they are not sufficient to specify an individual member of the family.

The requirement that a new drug fill the active site pocket the way the Alrestatin double-decker does should lead to many interactions with the enzyme. Additionally, the bulkier shape of a drug that mimics the Alrestatin double-decker may minimize or obviate inhibition of other aldo−keto reductase family members for steric reasons. The requirement that a new drug recognize the C-terminal tail of aldose reductase should also improve the specificity of the drug. The next generation of aldose reductase inhibitors may resemble a derivative of a ferrocene molecule or two covalently linked Alrestatin molecules. Drugs that mimic the Alrestatin double-decker may thus represent a new class of specific inhibitors with little or no cross-reactivity and may have a wider utility in our pharmacological armamentarium.

NOTE ADDED IN PROOF

The conclusions reached by Urzhumtsev *et al.* (*25*) as to the nature of the specificity determinant of aldose reductase based upon the structures of bound Tolerastat and Sorbinil are largely consistent with those presented here.

REFERENCES

1. Harrison, D. H., Bohren, K. M., Ringe, D., Petsko, G. A., & Gabbay, K. H. (1994) *Biochemistry 33*, 2011−2020.
2. Wilson, D. K., Bohren, K. M., Gabbay, K. H., & Quiocho, F. A. (1992) *Science 257*, 81−84.
3. Bohren, K. M., Grimshaw, C. E., Lai, C. J., Harrison, D. H., Ringe, D., Petsko, G. A., & Gabbay, K. H. (1994) *Biochemistry 33*, 2021−2032.
4. Grimshaw, C. E., Bohren, K. M., Lai, C. J., & Gabbay, K. H. (1995) *Biochemistry 34*, 14356−14365.
5. Grimshaw, C. E., Shahbaz, M., & Putney, C. G. (1990) *Biochemistry 29*, 9947−9955.
6. Gabbay, K. H. (1975) *Ann. Rev. Med. 26*, 521−536.
7. Kador, P. F. (1988) *Med. Res. Rev. 8*, 325−352.
8. Dvornik, D. (1992) *J. Diabetes Complications 6*, 25−34.
9. Dvornik, E., Simard-Duquesne, N., Krami, M., Sestanj, K., Gabbay, K. H., Kinoshita, J. H., Varma, S. D., & Merola, L. O. (1973) *Science 182*, 1146−1148.
10. Gabbay, K. H., Spack, N., Loo, S., Hirsch, H. J., & Ackil, A. A. (1979) *Metab. Clin. Exp. 28*, 471−476.
11. Spielberg, S. P., Shear, N. H., Cannon, M., Hutson, N. J., & Gunderson, K. (1991) *Ann. Intern. Med. 114*, 720−724.
12. Martyn, C. N., Reid, W., Young, R. J., Ewing, D. J., & Clarke, B. F. (1987) *Diabetes 36*, 987−990.
13. Bohren, K. M., Page, J. L., Shankar, R., Henry, S. P., & Gabbay, K. H. (1991) *J. Biol Chem. 266*, 24031−24037.
14. Cleland, W. W. (1963) *Arch. Biochem. & Biophys. 67*, 104−137.
15. Kabsch, W. (1988) *J. Appl. Crystallogr. 21*, 916−924.
16. Brünger, A. T. (1993) *Computer Program X-PLOR*, Yale University Press, New Haven, CT.
17. Jones, T. A. (1991) *Acta Crystallogr. A47*, 110−119.
18. Wilson, D. K., Tarle, I., Petrash, J. M., & Quiocho, F. A. (1993) *Proc. Natl. Acad. Sci. U.S.A. 90*, 9847−9851.
19. Ehrig, T., Bohren, K. M., Prendergast, F. G., & Gabbay, K. H. (1994) *Biochemistry 33*, 7157−7165.
20. Barski, O. A., Gabbay, K. H., & Bohren, K. M. (1996) *Biochemistry 35*, 14276−14280.
21. Bohren, K. M., Grimshaw, C. E., & Gabbay, K. H. (1992) *J. Biol. Chem. 267*, 20965−20970.
22. Barski, O. A., Gabbay, K. H., Grimshaw, C. E., & Bohren, K. M. (1995) *Biochemistry 34*, 11264−11275.
23. Potier, N., Barth, P., Tritsch, D., Biellmann, J. F., and Van Dorsselaer, A. (1997) *Eur. J. Biochem. 243*, 274−282.
24. Genetics Computer Group (GCG) (1982) *Computer Program*, Wisconsin Package.
25. Urzhumtsev, A., Tete-Favier, F., Mitschler, A., Barbanton, J., Barth, P., Urzhumtseva, L., Biellmann, J. F., Podjarny, A., and Moras, D. (1997) *Structure 5*, 601−612.

BI9717136